Journal of Power Sources 196 (2011) 10775–10781

Contents lists available at SciVerse ScienceDirect

Journal of Power Sources

journal homepage: www.elsevier.com/locate/jpowsour

# Electrochemical properties of graphene nanosheets/polyaniline nanofibers composites as electrode for supercapacitors

Jing Li, Huaqing Xie*, Yang Li, Jie Liu, Zhuxin Li

*School of Urban Development and Environmental Engineering, Shanghai Second Polytechnic University, Shanghai 201209, PR China*

ARTICLE INFO

*Article history:*
Received 5 July 2011
Received in revised form 25 August 2011
Accepted 26 August 2011
Available online 2 September 2011

*Keywords:*
Graphene
Polyaniline nanofiber
Composite
Supercapacitor

ABSTRACT

Graphene nanosheets/polyaniline nanofibers (GNS/PANI) composites are synthesized via in situ polymerization of aniline monomer in $HClO_4$ solution. The PANI nanofibers homogeneously coating on the surface of GNS greatly improve the charge transfer reaction. The GNS/PANI composites exhibit better electrochemical performances than the pure individual components. A remarkable specific capacitance of 1130 F $g^{-1}$ (based on GNS/PANI composites) is obtained at a scan rate of 5 mV $s^{-1}$ in 1 M $H_2SO_4$ solution compared to 402 F $g^{-1}$ for pure PANI and 270 F $g^{-1}$ for GNS. The excellent performance is not only due to the GNS which can provide good electrical conductivity and high specific surface area, but also associate with a good redox activity of ordered PANI nanofibers. Moreover, the GNS/PANI composites present excellent long cycle life with 87% specific capacitance retained after 1000 charge/discharge processes. The resulting composites are promising electrode materials for high-performance electrical energy storage devices.



## 1. Introduction

Supercapacitors are efficient electrical energy storage and have attracted considerable attention during the past decades because of their advantages over conventional dielectric capacitors. There are two mechanisms to store energy [1], namely ion adsorption (electrical double layer capacitance, EDLC), and reversible faradaic reactions (pseudocapacitance). Carbon-based materials with good electrical conductivity and high specific surface area are usually adopted as electrode materials for electrical double layer capacitors (EDLCs). The conducting polymers and metal oxides are usually used as pseudocapacitors or redox supercapacitors electrode materials. To further enhance the specific capacitance of supercapacitors, the pseudocapacitance can be coupled with the EDLC depending on the nature of the electrode [2,3].

Graphene, a new carbonous material with two-dimensional (2D) nanostructure, has attracted great attention both in fundamental science and applied research [4]. Owing to its exceptional thermal stability [5], optimal mechanical stiffness [6], excellent electronic properties and electrical conductivity [7], graphene has been proposed for potential applications in electronics and transistors [8,9]. Up to now, many methods have been developed to synthesize graphene, including mechanical cleavage [10], thermal exfoliation [11], chemical exfoliation [12] of graphite, epitaxial growth on SiC [13] and unzipping carbon nanotubes [14]. In electrochemical measurements, multilayer graphene with different layers from two to ten or more, are considered to be promising electrode materials for supercapacitors, lithium batteries, solar cells, and hydrogen storage [15–18]. Great effort has also been devoted to compounding graphene with polymers or inorganic particles to synthesize composites [19,20].

Among the conducting polymers, polyaniline (PANI) is considered to be the most promising electrode material for supercapacitors due to its excellent capacity for energy storage, easy synthesis, high conductivity, and low cost [21]. However, PANI is susceptible to rapid degradation in performance upon repetitive cycles (charge/discharge process) because of its swelling and shrinkage. In order to alleviate this limitation, the combination of PANI with carbon materials has been proved to reinforce the stability of PANI as well as maximize the capacitance value [22,23]. Due to the intriguing properties of graphene and the advantages of PANI, composites of graphene and PANI have exhibited great promise as supercapacitors electrode materials due to the conductivity, high surface area and the ability to store energy via two charge storage mechanisms. Recently, several researches have been reported on incorporating graphene into PANI matrices to produce nanocomposites for supercapacitors electrode. However, the specific capacitance is low, about 111 F $g^{-1}$ for graphene [24] and 233 F $g^{-1}$ for graphene/PANI composites [25]. The capacitance of graphene/PANI composites is mainly dominated by the

* Corresponding author. Tel.: +86 21 50217331; fax: +86 21 50217331.
*E-mail address:* hqxie@eed.sspu.cn (H. Xie).

0378-7753/$ – see front matter © 2011 Elsevier B.V. All rights reserved.
doi:10.1016/j.jpowsour.2011.08.105

pseudocapacitance from the PANI. The EDLC for graphene is not high possibly due to agglomerated layer-like structure of graphene sheets [26]. Thus, it is important to control graphene as thin as possible and disperse it homogeneously in the composites matrix.

In this work, composites of graphene nanosheets/polyaniline nanofibers (GNS/PANI) with different mass ratios are synthesized by in situ polymerization of aniline monomer in the presence of graphene suspension in $HClO_4$ solution. The introduction of amounts of GNS into PANI nanofibers could greatly enhance the electrochemical performances of composites. The GNS/PANI composites exhibit high specific capacitance (1130 F $g^{-1}$) at a scan rate of 5 mV $s^{-1}$ and excellent long-term cycle stability (87% retention life after 1000 cycles). The morphology, microstructure and electrochemical performances of the GNS/PANI composites have been investigated. The influence of mass ratio on the specific capacitance is also evaluated.

## 2. Experimental

### 2.1. Synthesis of GNS/PANI composites

Aniline was distilled under the protection of high purity $N_2$ and then kept in a refrigerator before use. All the other chemicals were analytical reagent and used without further purification. Graphite oxide was synthesized using natural graphite oxidation by the modified Hummers method [27]. GNS was prepared by the reduction of graphene oxide (GO) with hydrazine as described elsewhere [28].

Homogenous composites of GNS/PANI with different mass ratios were synthesized through in situ polymerization of aniline monomer in the presence of graphene suspension. The mass ratio of GNS to aniline is varied as 1:99, 6:94, 20:80, and signed as $GP_{ratio}$, like $GP_{1:99}$, indicating the mass ratio of GNS and aniline is 1:99. The typical route is as follows, for example, when the mass ratio is 6:94. First, the purified aniline (10.1 mmol) was added into 30 mL GNS suspension (2 mg $mL^{-1}$). The mixture of aniline and GNS was obtained after ultrasonication for 30 min. While maintaining vigorous stirring at room temperature, ammonium persulfate (APS, 2.5 mmol) in 30 mL of 2 M $HClO_4$ solution was rapidly poured into the above mixture. Polymerization of aniline started after about 5 min, and then the reaction was allowed to stir overnight. The mixture was diluted by 200 mL of deionized water. The precipitated composite was collected by filtration and repetitively washed with water until the filtrate became colorless, dried at 60 °C for 12 h in a vacuum oven. For comparison, pure PANI was also synthesized through the above mentioned chemical process without the presence of GNS suspension. After having been dried under vacuum at 60 °C for 12 h, the PANI powder is obtained.

To evaluate the yield of dedoped PANI, the synthesized PANI nanofibers were dispersed in 2 M ammonia water for more than 48 h in amagnetic stirrer for complete dedoping. The product was filtered and rinsed with distilled water until the filtrate became neutral. After having been dried under vacuum at 60 °C, the final dedoped PANI powder was collected with a yield of 25%. The same procedure was used to evaluate yields of dedoped PANI in the composites. The yields are estimated as 28% for $GP_{1:99}$, 30% for $GP_{6:94}$, and 28% for $GP_{20:80}$ by adding the same amount of aniline in the reaction system. The main drawback of the polymerization for preparation of PANI nanofibers is the low concentration of aniline and hence lower yield of PANI nanofibers [29,30]. The molar ratio of APS/aniline and concentration of aniline monomer has a significant effect on the yield of PANI nanofibers [31]. The results indicate that the GNS has a positive effect on the polymerization of aniline monomer, which can provide much more active sites for nucleation of aniline molecules.

### 2.2. Characterization methods

The microstructure and morphologies of the samples were investigated by a scanning electron microscopy S-4800 (SEM, HITACHI) and transmission electron microscopy 2100F (TEM, JEOL). Atomic force microscopic (AFM) image was taken on Scanning Probe Microscope SPM-9600 Series (SHIMADZU CORPORATION, Japan). XRD measurements were recorded on X-ray diffraction system (D8-Advance, Germany) equipped with Cu Kα radiation (λ = 1.54 Å). Nitrogen adsorption–desorption isotherms were measured at 77 K using Micromeritics (NOVA 4200e) analyzer after heating the sample at 100 °C for 2 h. The Brunauer–Emmett–Teller (BET) surface area of the samples was measured using nitrogen adsorption data over a relative pressure ranging from 0.05 to 0.3.

### 2.3. Preparation of electrodes and electrochemical measurements

A glassy carbon electrode (GCE, Ø 4 mm) was used as the substrate to prepare the samples modified electrode. GCE was carefully polished with alumina powders (0.3 and 0.05 μm) on a polishing cloth, rinsed thoroughly with deionized water between each polishing step, sonicated in ethanol and water, and then allowed to dry at room temperature. The working electrode was prepared by casting a nafion-impregnated sample onto GCE surface. Typically, 10 mg of the sample was dispersed in 5 mL of ethanol containing 10 μL of nafion (5 wt% in ethanol) by ultrasonication for 30 min. 10 μL of the treated suspension was dripped onto the GCE surface, naturally dried at room temperature to form the sample adsorbed GCE. The thickness of the film can be controlled based on the amount of the dripping suspension. 500 nm thickness of the film is generated on the electrode. Such a thin composite electrode may be favorable for the enhancement of the electrochemical performances for supercapacitors.

The electrochemical tests were carried out in $H_2SO_4$ aqueous electrolyte solution at room temperature. A three-electrode system was used, consisting of the sample modified GCE as the working electrode, platinum as the counter electrode, and a saturated calomel electrode (SCE) as the reference electrode. Cyclic voltammetry (CV) and electrochemical impedance spectroscopy (EIS) were performed with a CHI 660C electrochemical workstation (ChenHua Instruments Co., Shanghai, China). EIS was recorded in the frequency range from $10^5$ to 0.1 Hz at open circuit potential with an AC voltage amplitude of 5 mV. Galvanostatic charge/discharge curves were measured in a voltage range from 0 to 0.80 V, using computer controlled cycling equipment (LAND, Wuhan China).

## 3. Results and discussion

### 3.1. Microstructure characterizations

The surface morphology and microstructure of the samples are examined. Fig. 1 displays the AFM image of GO sheets. The cross-section analysis in the AFM height image shows the thickness is ~1.1 nm, indicating the full exfoliation of graphite oxide [32]. After reduction by hydrazine, GNS exhibit a wrinkled morphology. As shown in Fig. 2a, large sheets of graphene with transparent in-plane morphology are observed on the top of the grid, reflecting its lamellar microstructure. Some of graphene are folded at the edge of sheets. Fig. 2b depicts the HRTEM image of graphene edges. The thickness of the edge of sheets is about 2–2.5 nm and is composed of approximately 3–4 wrinkled individual monoatomic graphene layers. The slightly crumpled and rippled structure morphology of the sheets may indicate that GO have not been entirely reduced to graphene. GO contains a wide range of oxygen functional groups

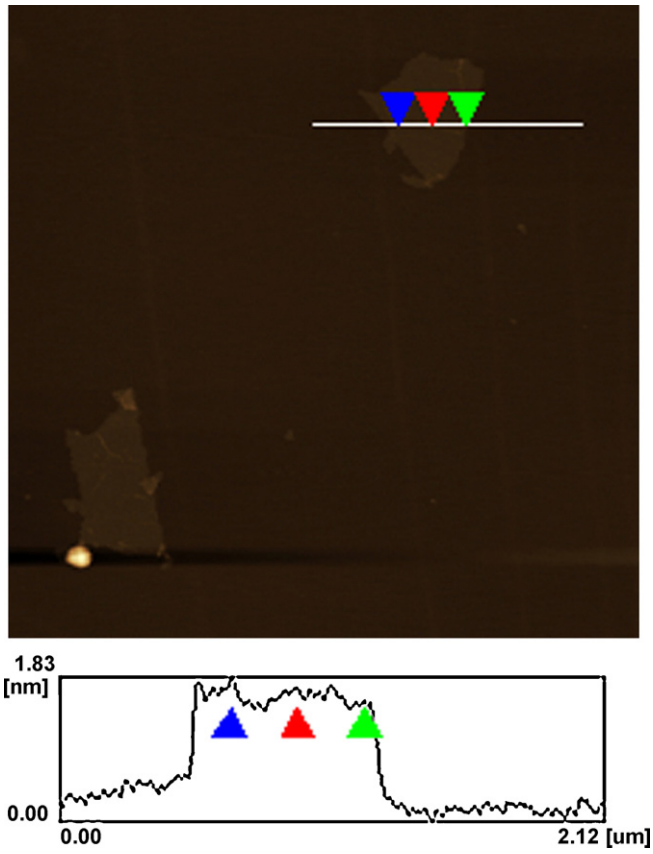


**Fig. 1.** AFM image of exfoliated GO sheets on mica surfaces with height profiles.

such as hydroxyl, epoxide, carboxyl, and carbonyl. The X-ray photoelectron spectroscopy (XPS, data was not shown) indicates that the O/C ratio in the exfoliated GO decreases remarkably after hydrazine reduction process, and that most of oxygen containing functional groups are significantly reduced. In addition, the oxygen content decreases to about 8% in GNS, which is in accordance with the literature reported [33]. The pure PANI exhibits uniform fibrous structures of hundreds of nanometers in length and 50 nm in width (Fig. 2c). Fig. 2d presents the image of $GP_{6:94}$ composites, in which PANI nanofibers with diameter of 50 nm along with GNS. GNS are used as support materials for the polymerization of PANI, and thus would be beneficent to improve the conductivity of the composites.

The morphology of PANI and GNS/PANI composites is also analyzed by SEM. The pure PANI shows nanofiber morphology with a diameter of about 50 nm (Fig. 3a), where they seem to be more compact and obtain a relatively shorter network structure. As for the GNS/PANI composites (Fig. 3b), PANI nanofibers on the order of 50 nm have been grown on GNS surface. Because of the nanofibrillar morphology and high overall coverage of PANI, the layered structure of GNS cannot be observed clearly. Rapid chemical reaction can promote homogeneous nucleation of growing PANI chains and thus form uniform nanofibers [34]. GNS bring negative charges due to their residual carboxylic groups [35]. Therefore, it is expected that aniline monomer can be adsorbed to the surface of GNS under ultrasonication. When APS are added into the suspension, the aniline molecules are initiated to polymerize just from the absorbed sites on the GNS surface, and then the nanofiber structure of PANI covering GNS nanosheet gradually forms. Hence, the GNS is considered as support material which can provide a large number of active sites for nucleation of aniline [36]. Since the capacitive performances of electrode materials are strongly dependent on their microstructures, the fibrous network of both PANI and the composites are believed to be desirable for the applications in supercapacitors.

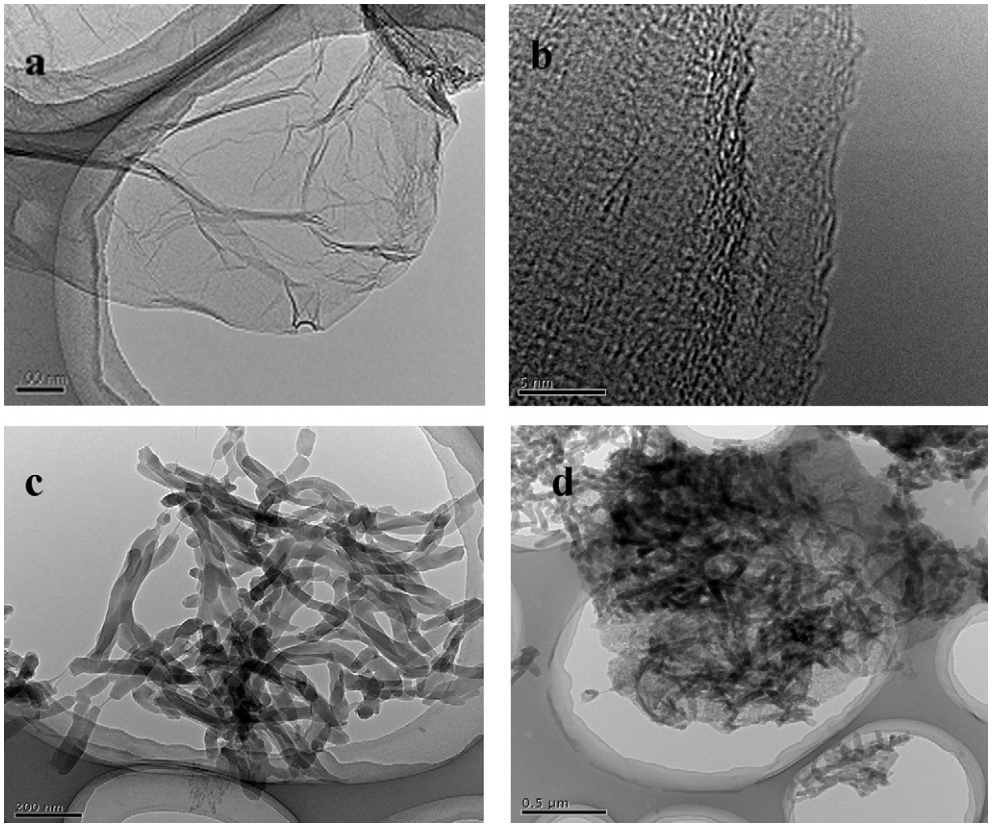


**Fig. 2.** TEM images of (a) GNS, (b) HRTEM image of GNS, (c) PANI nanofibers and (d) GNS/PANI composites.

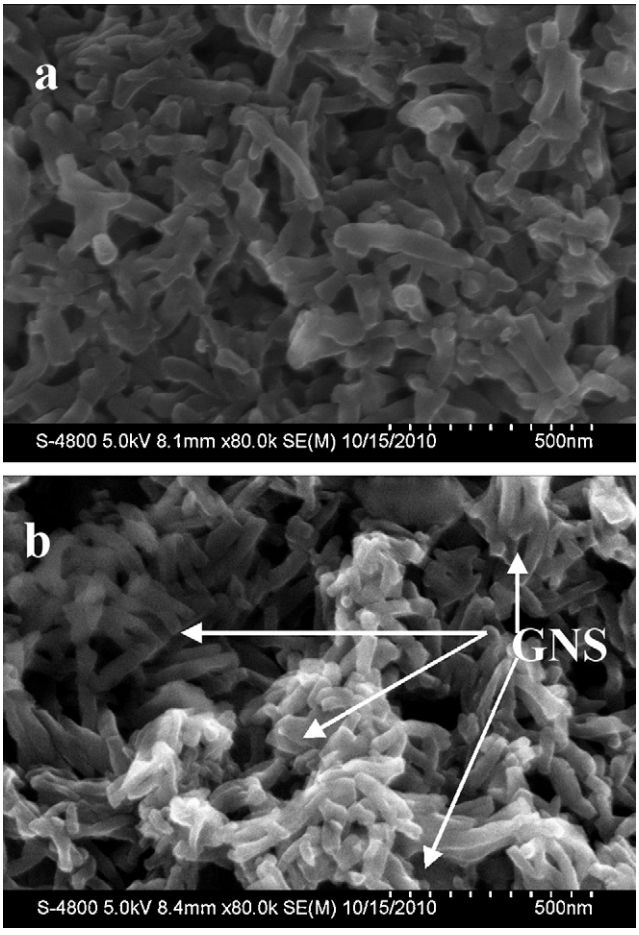


**Fig. 3.** SEM images of PANI nanofibers (a) and GNS/PANI composites (b).

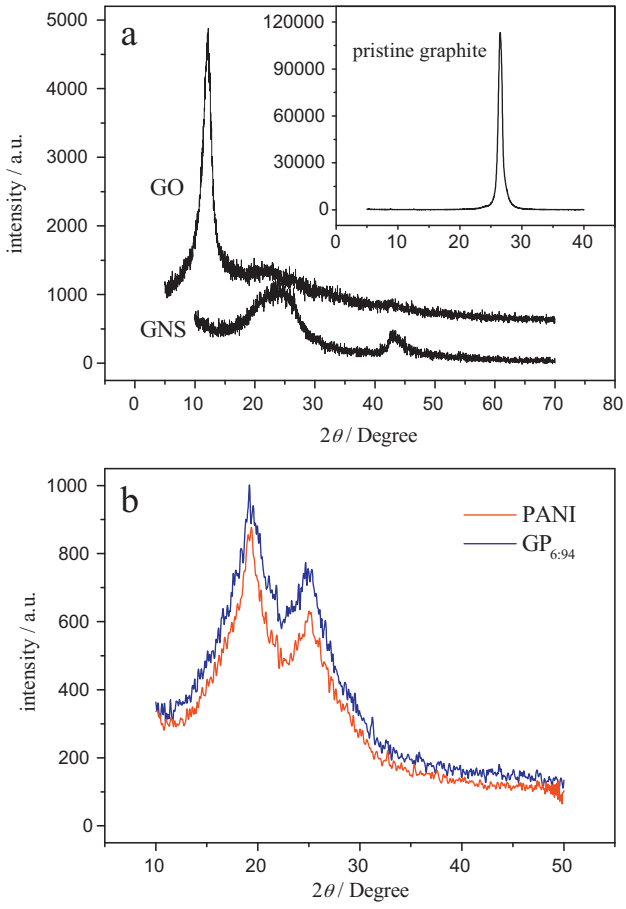


**Fig. 4.** (a) XRD patterns of pristine graphite, GO and GNS, (b) individual PANI and $GP_{6:94}$ composites.

Fig. 4 represents the XRD patterns of pristine graphite, GO, GNS, pure PANI and GNS/PANI composites, respectively. As shown in Fig. 4a, pristine graphite reveals a sharp (0 0 2) diffraction peak at $2\theta = 26.4^\circ$. The pattern has not presented in the GO which has a diffraction peak at 12.1°, because the chemical oxidation would disrupt the ordering of layers and introduce functional groups containing oxygen to the graphite. The interlayer spacing of GO layers (0.733 nm) is much larger than that of pristine graphite (0.335 nm), implying the exfoliation of graphite [37]. GNS exhibits a broad diffraction peak for C (0 0 2) at $2\theta = 24.1^\circ$, corresponds to an interlayer spacing of 0.368 nm, which is slightly higher than that of well-ordered natural graphite. The result can be interpreted the presence of residual functional groups containing oxygen in graphene layers. For the pure PANI with $HClO_4$ as dopant (Fig. 4b), two peaks appear at 19.3° and 25.2°, corresponding to (0 2 0) and (2 0 0) crystal planes of PANI in its emeraldine salt state [38]. As the GNS mass percentage increases in the composites, the composites present crystalline peaks similar to that observed from individual PANI. However, the diffraction peak of GNS at 42.8° disappears, implying that the PANI and GNS have been completely interacted.

The specific surface area of GNS is calculated by BET method and the value is 288.9 $m^2\ g^{-1}$. This high value is partially attributed to a degree of GO exfoliation prior to the reduction. The BET surface area of $GP_{1:99}$ (43.8 $m^2\ g^{-1}$) and $GP_{6:94}$ (56.5 $m^2\ g^{-1}$) are much larger than that of pure PANI (25.8 $m^2\ g^{-1}$). The BET surface area of the samples has an obvious enhancement with increasing the GNS content, assigned to the larger fraction of GNS in the composites. However, the surface area of $GP_{20:80}$ is only 29.6 $m^2\ g^{-1}$, which may be due to the high content of GNS would affect the growth of PANI nanofibers. These results mean that introduce less content of GNS into PANI matrix can effectively increase the surface area, resulting in the high electrochemical utilization of PANI and graphene sheets.

### 3.2. Electrochemical behavior

In order to evaluate the electrochemical properties of the electrode materials, CV tests, galvanostatic charge/discharge and EIS were employed to characterize the capacitance performances. The specific capacitance of the electrode can be calculated according to the following equation from CV curves:

$$C = \int \frac{I\ dV}{vmV} \quad (1)$$

where $C$ is the specific capacitance based on the mass of electroactive materials ($F\ g^{-1}$), $I$ is the response current (A), $V$ is the potential (V), $v$ is the potential scan rate ($V\ s^{-1}$), and $m$ is the mass of the active electrode materials (g).

Fig. 5a illustrates the CVs of GO, GNS, PANI and GNS/PANI composites at a scan rate of 5 $mV\ s^{-1}$ in 1 M $H_2SO_4$ solution. The curves of GO and GNS electrodes exhibit an approximately rectangular shape which is characteristic of an EDLC. In a significant difference from GO and GNS electrodes, both the PANI and GNS/PANI composites electrodes exhibit two pairs of redox waves ($C_1/A_1$, $C_2/A_2$) which are indicative of a typical pseudocapacitive characteristic of PANI. Peaks of $C_1/A_1$ are ascribed to the redox transition of PANI from a semiconducting state (leucoemeraldine form) to a conducting state (emeraldine form). Faradaic transformation from

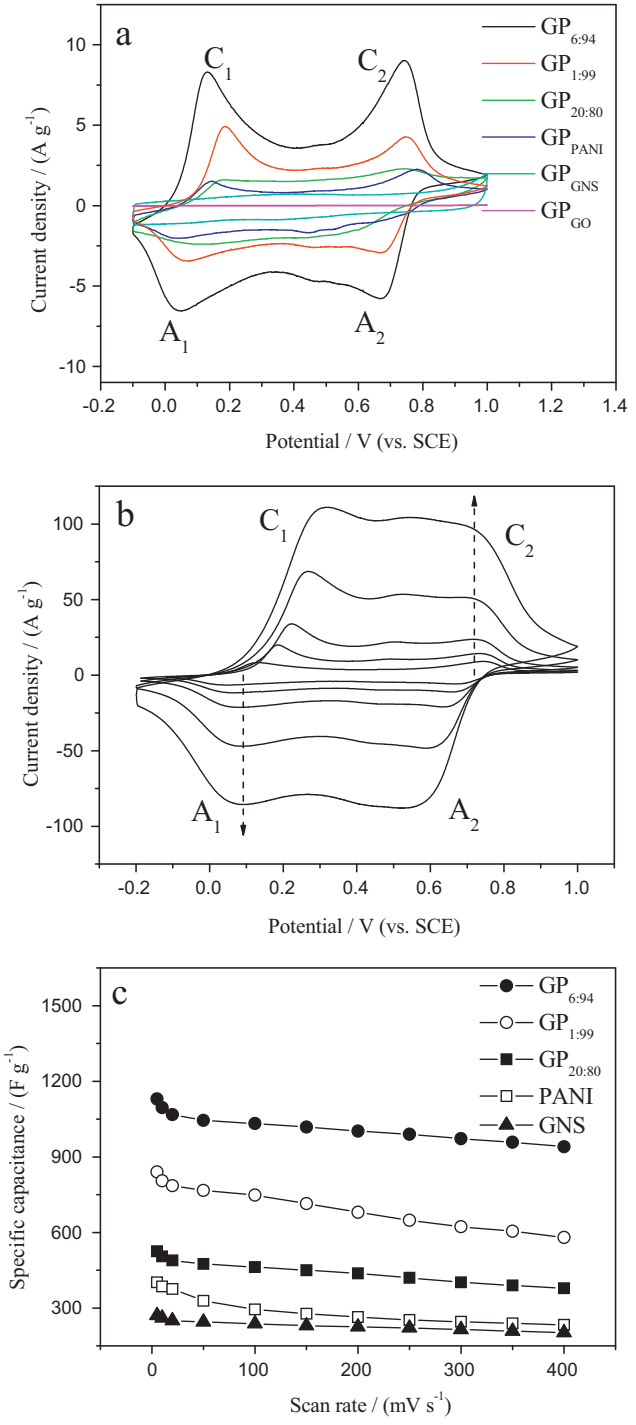


**Fig. 5.** (a) CV curves of GO, GNS, PANI and GNS/PANI composites at 5 mV $s^{-1}$ in 1 M $H_2SO_4$ solution, (b) CV curves of $GP_{6:94}$ at different scan rates of 5, 10, 20, 50 and 100 mV $s^{-1}$. The arrow indicates the increase of the scan rates from 5 to 100 mV $s^{-1}$, (c) specific capacitance of GNS, PANI and GNS/PANI composites at different scan rates.

emeraldine to pernigraniline is responsible for peaks of $C_2/A_2$ [39]. The voltammetric curves of the GNS/PANI composites electrode present behavior of a combination of both redox capacitance and EDLC. It can be apparently found that the surrounded by CV curves of GNS/PANI composites is apparently larger than that of pure PANI, indicating higher specific capacitance. Besides, the capacitive performances of GNS/PANI composites are enhanced to different degrees as the mass ratio changes. The diffusion length ($L$) of electrolyte ions within the electrode during the charge/discharge process can be estimated as $(Dt)^{1/2}$ [39], where $D$ and $t$ are the diffusion coefficient and time, respectively. The nanometer-sized PANI provides enhanced electrode/electrolyte interface areas, which can enable the electrochemical accessibility of electrolyte through the loosely packed PANI fibrous structure. Furthermore, the GNS in the composite can not only offer highly conductive path, but also serve as a high surface area support material for the polymerization of PANI, facilitating rapid transport of the electrolyte ions in the electrode during rapid charge/discharge processes. Therefore, the composites can greatly reduce the diffusion length, resulting in the improvement of electrochemical properties of GNS/PANI composites materials. More interestingly, the CV shapes of different GNS/PANI composites have a little change. The CV behavior actually exhibits the synergetic performance of PANI and GNS, which may influence the shape and potential position of curves.

Fig. 5b shows the CV curves of $GP_{6:94}$ at different scan rates. It is notable that the synthesized materials exhibit excellent electrochemical behavior in a wide range of scan rates. It can be also observed that the oxidation peaks ($C_1$ and $C_2$) shift positively and the reduction peaks ($A_1$ and $A_2$) shift negatively with increasing potential sweep rates, which is mainly due to the resistance of the electrode [39]. Between 5 and 200 mV $s^{-1}$, the scan rate dependence of the peak current was investigated on the first redox waves of PANI. The peak currents evolve linearly with the square root of the scan rates, indicating diffusion limited redox process, which is in accordance of the electrochemical processes of polycarbazole films [40]. Similar results were observed for composites of $GP_{1:99}$ and $GP_{20:80}$. Additionally, the obvious increase of peak current density with improving the scan rates indicates good rate ability for GNS/PANI composites electrode.

Fig. 5c displays the relationship of specific capacitance of the synthesized electrode materials and scan rates. The specific capacitance of GNS/PANI composites is much higher than that of pure GNS and PANI at the same scan rates. The maximum specific capacitance of 1130 F $g^{-1}$ is obtained at a scan rate of 5 mV $s^{-1}$ for $GP_{6:94}$, compared to 270, 402, 840 and 525 F $g^{-1}$ for GNS, pure PANI, $GP_{1:99}$ and $GP_{20:80}$, respectively. Even at 400 mV $s^{-1}$, the specific capacitance of $GP_{6:94}$ still presents 940 F $g^{-1}$, while only 233 F $g^{-1}$ for pure PANI. The greatly enhanced specific capacitance for GNS/PANI composites is probably due to the synergetic effect between the two components. The well-ordered PANI nanofibers on GNS not only effectively inhibit the stacking/agglomerating of GNS, resulting in high EDLC, but also exhibit enhanced electrode/electrolyte interface areas, improving the high electrochemical utilization of PANI. Furthermore, GNS in the composites also provide highly conductive path for electron transport during the charge/discharge processes.

The galvanostatic charge/discharge is a reliable method to evaluate the electrochemical capacitance of materials under controlled current conditions. Fig. 6 demonstrates the curves of the samples tested at a current density of 2.5 A $g^{-1}$ for the initial three cycles. The GNS electrode shows a triangular-shape charge/discharge curve, indicating its capacitance is mainly due to an EDLC. Galvanostatic charge/discharge plots of PANI and GNS/PANI ($GP_{6:94}$) composites present a capacitive behavior with almost symmetric charge/discharge curves. Moreover, the deviation to linearity is typical of a pseudocapacitive contribution. The excellent specific capacitive ability of the GNS/PANI composites electrode owes to the multi-state of PANI. Although the charge/discharge curves of PANI nanofibers maintain the similar shape of the GNS/PANI composites, the "IR drop" of PANI electrode is much higher than that of $GP_{6:94}$ composites, reflecting the internal resistance of PANI is much higher than that of the composites. Low internal resistance is important in energy storage devices. Less energy will be wasted to produce unwanted heat during charge/discharge processes [41].

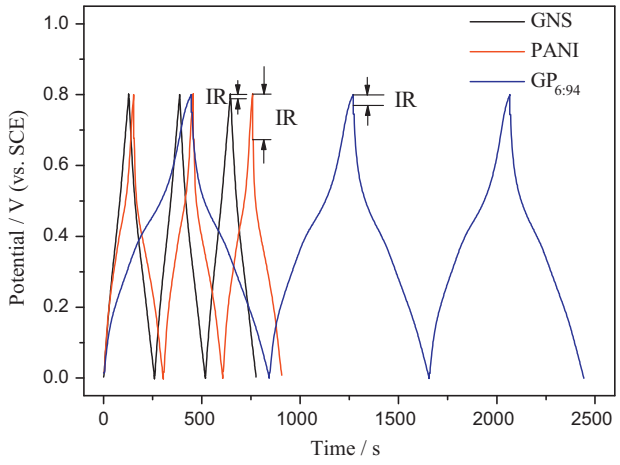


**Fig. 6.** Galvanostatic charge/discharge measurements of the electrode materials within the potential window of 0–0.80 V (vs. SCE) at a current density of 2.5 A $g^{-1}$.

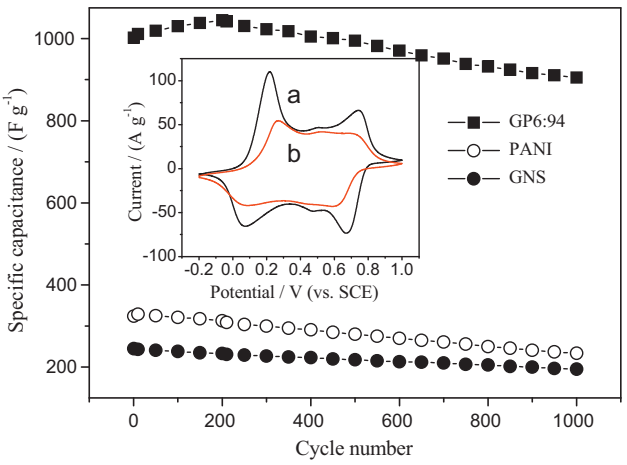


**Fig. 8.** Variation of the specific capacitance of pure PANI, GNS and $GP_{6:94}$ composite electrodes as a function of cycle number measured at 50 mV $s^{-1}$ in 1 M $H_2SO_4$ aqueous solution. Inset shows the 1st (curve a) and the 1000th (curve b) CVs of the $GP_{6:94}$ composite.

The good conductivity of GNS has low internal resistance and exhibits large surface area. In addition, the charge/discharge duration increases in the order of pure GNS < PANI < $GP_{6:94}$, implying the highest specific capacitance for GNS/PANI composites. These results are in accordance with those deduced from the CV measurements.

The EIS analysis is a powerful and informative technique to evaluate the properties of conductivity, structure and charge transport in the film/electrolyte interface. The Nyquist plots of pure GNS, PANI and $GP_{6:94}$ are displayed in Fig. 7. It is apparent that the plot of pure PANI presents a single semicircle in the high-frequency region and a straight line in the low-frequency region. The diagrams of GNS and $GP_{6:94}$ do not present semicircle at high-frequency, probably due to the low faradaic charge transfer resistances. The $GP_{6:94}$ composites electrode exhibits a more vertical line than PANI and GNS at low-frequency, illustrating better capacitive behavior and lower diffusion resistance of ions. The intersection of the curves at the real axis in the range of high-frequency represents solution resistance ($R_s$). The $R_s$ of $GP_{6:94}$ is about 0.8 Ω, which is much smaller than that of PANI (1.5 Ω). The decreased $R_s$ of $GP_{6:94}$ composite may be attributed to the doping process and π–π stacking between GNS and PANI, in which the structure can facilitate the efficient access of electrolyte ions to the electrode surface and shorten the ion diffusion path.

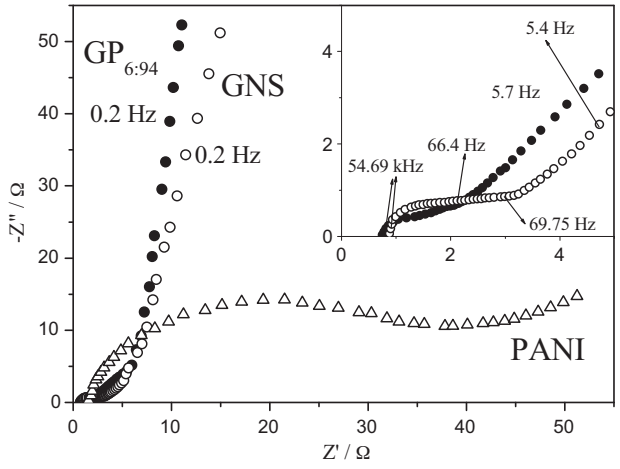


**Fig. 7.** Impedance spectra of pure PANI, GNS and the composite of $GP_{6:94}$ in 1 M $H_2SO_4$ solution measured at open circuit potential.

### 3.3. Stability and reproducibility

Long cycle life is a crucial parameter for supercapacitors electrode materials. The electrochemical stability of pure GNS, PANI and $GP_{6:94}$ composites was evaluated by repeating the CV test between −0.2 and 1.0 V at a scan rate of 50 mV $s^{-1}$ for 1000 cycles. The CV curves of $GP_{6:94}$ composites before charge/discharge test and after 1000 cycles are shown in Fig. 8 (inset). The CV curve with two pairs of evident redox peaks is observed at first cycle, indicating the electrode has both EDLC and pseudocapacitance. After 1000 cycles, the redox peaks become weak, which is attributed to reduced pseudocapacitance of PANI. The specific capacitance of the electrode materials as a function of cycle number is presented in Fig. 8. The $GP_{6:94}$ electrode exhibit excellent long cycle life in the entire cycle numbers. Interestingly, the specific capacitance increases first for the 1–200 cycles and then maintain approximately steady, indicating the electrode is fully activated and reach the optimum condition. After 1000 cycles, the capacitance decreases only 13% of initial value compared to 20% and 29% for GNS and PANI, demonstrating the GNS/PANI composites electrode has long-term electrochemical stability. These results reveal that GNS in the composites could improve the service life of PANI. The decrease of the specific capacitance probably results from swelling and shrinkage of conducting PANI, which may lead to degradation of the polymeric conductivity and charge storage capability during charge/discharge processes. After several hundreds of cycles, the interaction force between GNS and PANI remained unchanged, implying that the transfer ability of charges would remain fairly constant.

The reproducibility of the electrochemical capacitances of GNS, PANI and $GP_{6:94}$ composites are also tested by repetitive recording of CVs in $H_2SO_4$ solution. It is found that the relative standard deviation (R.S.D.) of the specific capacitance for 20 replicate determinations is 3.3%, 3.6% and 3.1%, respectively. Ten pieces of the proposed electrode are prepared and the R.S.D. for the individual determination is 3.2%, 3.3% and 2.9%, respectively. These results demonstrate that fabricated supercapacitors electrodes have excellent reproducibility.

## 4. Conclusions

In summary, GNS/PANI composites have been synthesized using in situ polymerization. The introduction of GNS into the composites provides a relatively large surface area for dispersing PANI

nanofibers, which can effectively enhance the kinetic for both charge transfer and ion transport throughout the electrode. The maximum specific capacitance is 1130 F $g^{-1}$ (based on $GP_{6:94}$ composite) at a scan rate of 5 mV $s^{-1}$ in 1 M $H_2SO_4$ solution. After 1000 charge/discharge processes, the specific capacitance maintains 87% of initial specific capacitance. The greatly enhanced specific capacitance is due to the synergic effect of the two components of GNS and PANI nanofibers. The GNS/PANI composites with high specific capacitance are quite suitable and promising electrode materials for supercapacitors.

## Acknowledgements

This work was supported by the Shanghai Municipal Education Commission and the Shanghai Educational Development Foundation (11CG64), the Program for New Century Excellent Talents in University (NCET-10-883), the Program for Professor of Special Appointment (Eastern Scholar) at Shanghai Institutions of Higher Learning and Fundamental and priority program of Shanghai Committee of Science and Technology (10JC1405700).

## References

[1] B.E. Conway, Electrochemical Supercapacitors: Scientific Fundamentals and Technological Applications, Kluwer Academic/Plenum Press, New York, 1999.
[2] J. Yan, Z.J. Fan, T. Wei, J. Cheng, B. Shao, K. Wang, L.P. Song, M.L. Zhang, J. Power Sources 194 (2009) 1202–1207.
[3] Y.P. Fang, J.W. Liu, D.J. Yu, J.P. Wicksted, K. Kalkan, C.O. Topal, B.N. Flanders, J.D. Wu, J. Li, J. Power Sources 195 (2010) 674–679.
[4] K.S. Novoselov, A.K. Geim, S.V. Morozov, D. Jiang, M.I. Katsnelson, I.V. Grigorieva, S.V. Dubonos, A.A. Firsov, Nature 438 (2005) 197–200.
[5] A.M. Silva, M.S. Pires, V.N. Freire, E.L. Albuquerque, D.L. Azevedo, E.W.S. Caetano, J. Phys. Chem. C 114 (2010) 17472–17485.
[6] X.L. Wang, H. Bai, Z.Y. Yao, A.R. Liu, G.Q. Shi, J. Mater. Chem. 20 (2010) 9032–9036.
[7] A.H. Castro Neto, F. Guinea, N.M.R. Peres, K.S. Novoselov, A.K. Geim, Rev. Mod. Phys. 81 (2009) 109–162.
[8] G.K. Dimitrakakis, E. Tylianakis, G.E. Froudakis, Nano Lett. 8 (2008) 3166–3170.
[9] C.Y. Wang, D. Li, C.O. Too, G.G. Wallace, Chem. Mater. 21 (2009) 2604–2606.
[10] K.S. Novoselov, A.K. Geim, S.V. Morozov, D. Jiang, Y. Zhang, S.V. Dubonos, I.V. Grigorieva, A.A. Firsov, Science 306 (2004) 666–669.
[11] D.H. Deng, X.L. Pan, H. Zhang, Q.A. Fu, D.L. Tan, X.H. Bao, Adv. Mater. 22 (2010) 2168–2171.
[12] V.C. Tung, M.J. Allen, Y. Yang, R.B. Kaner, Nat. Nanotechnol. 4 (2009) 25–29.
[13] J.A. Robinson, C.P. Puls, N.E. Staley, J.P. Stitt, M.A. Fanton, K.V. Emtsev, T. Seyller, Y. Liu, Nano Lett. 9 (2009) 964–968.
[14] D.V. Kosynkin, A.L. Higginbotham, A. Sinitskii, J.R. Lomeda, A. Dimiev, B.K. Price, J.M. Tour, Nature 458 (2009) 872–876.
[15] L.L. Zhang, R. Zhou, X.S. Zhao, J. Mater. Chem. 20 (2010) 5983–5992.
[16] J.K. Lee, K.B. Smith, C.M. Hayner, H.H. Kung, Chem. Commun. 46 (2010) 2025–2027.
[17] L. Wang, K. Lee, Y.Y. Sun, M. Lucking, Z.F. Chen, J.J. Zhao, S.B.B. Zhang, ACS Nano 3 (2009) 2995–3000.
[18] Z.Y. Yin, S.X. Wu, X.Z. Zhou, X. Huang, Q.C. Zhang, F. Boey, H. Zhang, Small 6 (2010) 307–312.
[19] A.V. Murugan, T. Muraliganth, A. Manthiram, Chem. Mater. 21 (2009) 5004–5006.
[20] X. Zhao, Q.H. Zhang, D.J. Chen, P. Lu, Macromolecules 43 (2010) 2357–2363.
[21] R.H. Lee, H.H. Lai, J.J. Wang, R.J. Jeng, J.J. Lin, Thin Solid Films 517 (2008) 500–505.
[22] H. Tamai, M. Hakoda, T. Shiono, H. Yasuda, J. Mater. Sci. 42 (2007) 1293–1298.
[23] H.Y. Mi, X.G. Zhang, S.Y. An, X.G. Ye, S.D. Yang, Electrochem. Commun. 9 (2007) 2859–2862.
[24] A.P. Yu, I. Roes, A. Davies, Z.W. Chen, Appl. Phys. Lett. 96 (2010) 253105.
[25] D.W. Wang, F. Li, J.P. Zhao, W.C. Ren, Z.G. Chen, J. Tan, Z.S. Wu, I. Gentle, G.Q. Lu, H.M. Cheng, ACS Nano 3 (2009) 1745–1752.
[26] K. Zhang, L.L. Zhang, X.S. Zhao, J.S. Wu, Chem. Mater. 22 (2010) 1392–1401.
[27] W.S. Hummers, R.E. Offeman, J. Am. Chem. Soc. 80 (1958), 1339–1339.
[28] S. Stankovich, D.A. Dikin, R.D. Piner, K.A. Kohlhaas, A. Kleinhammes, Y. Jia, Y. Wu, S.T. Nguyen, R.S. Ruoff, Carbon 45 (2007) 1558–1565.
[29] J. Huang, S. Virji, B.H. Weiller, R.B. Kaner, J. Am. Chem. Soc. 125 (2003) 314–315.
[30] N.R. Chiou, A.J. Epstein, Adv. Mater. 73 (2005) 1679–1683.
[31] J. Qiang, Z. Yu, H. Wu, D. Yun, Synth. Met. 158 (2008) 544–547.
[32] Y.X. Xu, H. Bai, G.W. Lu, C. Li, G.Q. Shi, J. Am. Chem. Soc. 130 (2008) 5856–5857.
[33] X.B. Fan, W.C. Peng, Y. Li, X.Y. Li, S.L. Wang, G.L. Zhang, F.B. Zhang, Adv. Mater. 20 (2008) 4490–4493.
[34] A.Z. Sadek, W. Wlodarski, K. Kalantar-Zadeh, C. Baker, R.B. Kaner, Sens. Actuators A 139 (2007) 53–57.
[35] D. Li, M.B. Muller, S. Gilje, R.B. Kaner, G.G. Wallace, Nat. Nanotechnol. 3 (2008) 101–105.
[36] J. Yan, T. Wei, B. Shao, Z.J. Fan, W.Z. Qian, M.L. Zhang, F. Wei, Carbon 48 (2010) 487–493.
[37] T. Kyotani, H. Moriyama, A. Tomita, Carbon 35 (1997) 1185–1187.
[38] M. Deka, A.K. Nath, A. Kumar, J. Membr. Sci. 327 (2009) 188–194.
[39] Y.G. Wang, H.Q. Li, Y.Y. Xia, Adv. Mater. 18 (2006) 2619–2623.
[40] F. Tran-Van, T. Henri, C. Chevrot, Electrochim. Acta 47 (2002) 2927–2936.
[41] Q. Wu, Y.X., Z.Y. Yao, A.R. Liu, G.Q. Shi, ACS Nano 4 (2010) 1963–1970.